The Report Committee for Julia Katherine Day
Certifies that this is the approved version of the following report:

A Method for Modeling Under-Expanded Jets

APPROVED BY
SUPERVISING COMMITTEE:

Supervisor:

Erich A. Schneider

John R. Howell

A Method for Modeling Under-Expanded Jets

by

Julia Katherine Day, B.S.

Report

Presented to the Faculty of the Graduate School of

The University of Texas at Austin

in Partial Fulfillment

of the Requirements

for the Degree of

Master of Science in Engineering

The University of Texas at Austin

December 2012

Abstract

A Method for Modeling Under-Expanded Jets

Julia Katherine Day, MSE

The University of Texas at Austin, 2012

Supervisor: Erich Schneider

In nuclear power plants, a pipe break in the cooling line releases a jet that damages other equipment in containment, and is known as a loss of coolant accident (LOCA). This report specifically focuses on boiling water reactor (BWR) applications as a guide for future studies with pressurized water reactors (PWRs). This report presents a methodology for characterizing the jet such that, given a set of upstream conditions, the pressure field and damage potential of the jet can be predicted by an end user with a minimum of computation. The resultant model has many advantages over previous models in that it is easily calculated with knowledge readily available to plant operators and it provides new metrics that allow for a quick and intuitive understanding of the damage potential of the jet.

Table of Contents

List of Tables

List of Figures

Chapter 1: Introduction

Nuclear power plants require significant engineering work to prevent accidents and to ensure the safety of their workers, the surrounding communities and the environment. To this end, the safety standards and procedures of nuclear power plants are constantly reviewed and researched in order to improve engineering understanding and further reduce risks. It is only by anticipating and modeling possible accidents that the risks of such accidents are mitigated. Models must be justifiably conservative and rigorously scientific so that risk can be properly accounted for in the accident response procedures.

The accident type of interest to this study is the loss of coolant accident (LOCA). In this accident scenario, a pipe break in the cooling line releases a jet that then impinges on various pipes and other plant components in containment. This jet can damage the plant components, including the insulation on the surrounding pipes, which can result in debris that accumulates on the containment floor. Later in the plant response to the LOCA, the water on the floor of the containment is pumped through to feed the coolant line. The insulation debris on the containment floor can then block up the pump inlet, which both damages the pump and prevents the containment water from cooling the reactor.

Although there exist certain kinds of insulation that minimize this problem, not all existing power plants in the United States were built with them. Replacing the insulation is costly not only in terms of financial capital and lost plant output, but also radiation hazards to workers. When the plant is shut down to allow workers to replace insulation, there still exists incident radiation from the reactor that workers would be exposed to.

Even with proper management of personnel to reduce radiation exposure, there would still be a small health risk to the workers.

The specific type of nuclear power plant under study in this report is the pressurized water reactor (PWR). Unlike in a boiling water reactor (BWR) where the coolant water boils in the containment so that the hot leg of the cooling line contains steam, in a PWR the coolant water is pressurized so that it is maintained as liquid water all throughout the cooling system. The LOCA that occurs when a pipe break develops in a PWR cooling system results in a two-phase jet. This study focuses on the simpler case of a single-phase steam jet—as would occur in a BWR LOCA—with the future goal of expanding the study to the more complicated two-phase case.

As part of better understanding the risks in LOCA type accidents, characterizing the jet to better understand how it will affect and possibly damage plant components is imperative. The current methods assume that the insulation incurs damage at a given pressure impinged upon its surface. For this reason, the models have focused on the pressure fields—especially the stagnation pressure fields—of the jet as a correlate for the damage potential of the insulation. This report presents a methodology for characterizing the jet such that, given a set of upstream conditions, the pressure field and damage potential of the jet can be predicted by an end user with a minimum of computation.

Chapter 2: Background

Analytical Modeling

This study endeavors to model under-expanded compressible jet effects in both steam and air for application in nuclear power plants, and therefore much of the focus of the model will be on parameters of interest to that problem, e.g., pressure and shear fields in the jet. Most previous studies of under-expanded compressible jets, however, have focused on modeling and predicting other parameters. Also, although steam is the more relevant fluid for BWR and PWR applications, most other studies in this area have examined air, and thus it is a major focus for ease of comparison.

Historically, compressible jet effects have generally been of the most interest to aerospace applications and thus most studies have focused only on air jets. However, because air can be modeled as an ideal gas with minimal loss of accuracy, the addition of water vapor to this study has resulted in further complications that have not been extensively explored previously. Additionally, verifying experiments have generally been performed with air or other similar gases, further solidifying the necessity of verifying the current model with air.

In the study of compressible under-expanded jets, it has generally become customary to divide the jet into different axial regions for ease of study. These different regions have arisen from the varying physics of the flow in these regions, and thus are widespread in the literature. Throughout this study, these three regions will be described as the nearfield, midfield, and farfield regions.

Classical analysis of shock dynamics in under-expanded compressible jets is especially relevant to the nearfield solution, i.e., the region near the jet exit. The assumptions in this model include a flat velocity profile at the jet exit and no appreciable entropic effects except at the shocks. In the classical analysis model, an under-expanded

jet initially expands with isentropic Prandtl-Meyer expansion waves at the exit to equilibrate with the ambient pressure, increasing its velocity. When the jet meets the ambient air at the jet boundary, the jet reflects with an oblique shock that slows the flow and converges it toward the centerline. The jet then reflects with another oblique shock that diverges the flow toward the jet boundary. At the jet boundary, the jet expands, starting the entire process over again. This forms the familiar shock-diamond pattern, which will continue until the jet has gone through enough oblique shocks to reduce the flow velocity to the subsonic regime.

Thus, studies of nearfield effects have generally been based off of classical shock dynamics. However, one of the most significant inaccuracies of classical analysis in real world applications is its inherent assumption that the jet dynamics are isentropic except at the shocks. Thus, with each subsequent expansion and shock in the jet diamond pattern, the reality diverges farther from the classical model. The fact that small changes in the upstream conditions have significant effects on the initial expansion angles, which then affect subsequent shocks and Mach disks, only further complicates the problem. Because of these entropic complications, most studies focus only on the very nearfield effects near the jet exit or on the farfield effects after this complicated transitional midfield region has passed. Early studies especially focus on nearfield effects, paying close attention to the location of the first Mach disk.

One of the most important first studies is from Young, which analyzed experimental data from Ashkenas and Sherman to analyze the relationship between the nearfield entropy change in the jet and the location of the Mach disk. Ahead of the Mach disk, they considered entropy production due to rarefaction and behind the Mach disk, they considered entropy production due to molecular mixing. Entropy production at the Mach disk itself was analyzed as a normal shock. Their results found that the Mach disk

location was directly related to the square root of the ratio of the pressure at the jet exit p_0 to the ambient pressure p_a, was only weakly related to the ratio of specific heats of the gas and was not at all affected by the ratio of the jet exit temperature to the ambient temperature.

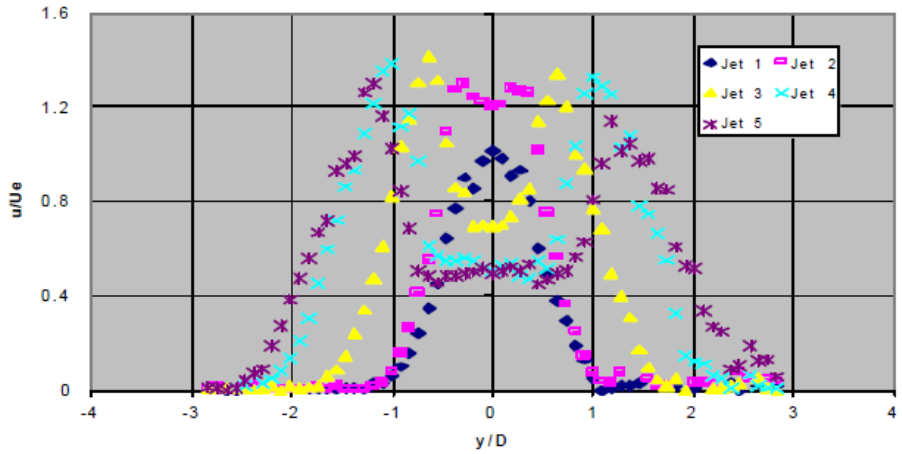

Figure 1. The effects of entrainment can be seen in the outer peaks that form around the middle peak, which is caused by jet expansion. The 5 jets shown above have varying jet Mach number, and the axial location is downstream of the first Mach disk. Taken in whole from Yüceil and Ötügen ("Underexpanded").

Many of the more recent studies have focused on the effects of turbulence and entrainment, especially as they relate to mixing enhancement in the nearfield region before and after the first Mach disk. In general, turbulent structures increase the momentum diffusion through turbulent convection, leading to quicker radial spread and velocity dissipation in the jet. Entrainment especially also significantly affects the radial velocity profile of the jet, as shown in Figure 1, which shows data from particle image velocimetry (PIV) experiments in underexpanded jets (Yüceil and Ötügen, "Underexpanded"). The temperature profiles would also presumably be affected, but this has not been a major area of study.

Gutmark, Schadow, and Yu provide a helpful review of turbulence and entrainment in under-expanded jets. Linear Stability Theory (LST) was used to relate the convective Mach number to the spreading rate of the shear layer, i.e., the region of entrained fluid at the jet boundary. The convective Mach number was defined by Bogdanoff to provide a measure of the effects of compressibility on turbulent convection, and is the ratio of the difference between the convection speed of the turbulent structures in the shear layer U_c and the speed in the freestream U normalized by the speed of sound in the freestream. Gutmark, Schadow, and Yu further explain that at low convective Mach numbers the shear layer acts as an incompressible shear layer, but as M_c increased above approximately 0.5, the mixing layer experiences increased instability, leading to a decrease in spreading rates. Experimentally, the decrease in spreading rates plateaus to an asymptotic value of 20% for M_c greater than approximately 0.9. Analytical studies using LST, however, predicted that the asymptotic value of the spreading rate should be 0. Various reasons have been proposed to explain this discrepancy, including the effects of three dimensional modes unaccounted for in LST (Groppengiesser), and the effects of the breakdown in the assumption of unbounded flows created by the existence of sidewalls (Soestrino).

Many of the more recent studies have begun to focus on farfield effects as a benchmark for jet similarity. Abramovich first proposed that at some significant axial distance from the jet source, all jets will become self-similar. This idea informs the basis of the asymptotic or farfield regime as the region of the jet where the jet has indeed become self-similar. The farfield can also be described as the region of the jet where the jet no longer experiences significant exchanges with the atmosphere. Experimental studies have shown quite conclusively that, in the farfield, the radial velocity profile of the jet is well approximated with a Gaussian distribution. As the jet continues along the

axis, the Gaussian curve flattens and expands as the jet slows and extends radially. It is assumed that at an infinite distance, the jet has dissipated completely into the atmosphere. Modeling these velocity dissipation and radial growth rates have been the focus of far-field effect studies. Similar attempts to model temperature have been made, although proposed correlations have general been unsuccessful at predicting jet behavior accurately.

Yüceil and Ötügen's work sets out to determine appropriate dimensionless parameters for predicting farfield jet behavior for under-expanded jets with a wide range of upstream conditions ("Scaling"). To this end, the authors of the study determined that the jet Mach number, which is defined as the Mach number that the theoretical perfectly and isentropically expanded jet would have at the same inlet conditions as the under-expanded jet being studied, was useful in determining useful parameters to collapse the velocity dissipation and radial growth rates. Experiments were performed to the data over a wide range of jet Mach numbers (from 1.0 to 3.3).

For the linear centerline velocity decay rate, the study determined in order to properly account for the fact that, although the jets issued from the same size nozzle, as *Mj* increased, so did the diameter of the subsequent jet similarly increase. Thus, the diameter of the same theoretical perfectly and isentropically expanded jet used to determine the jet Mach number, D_2, was used to normalize the downstream location x. A similar argument was used to justify the normalization of the centerline velocity V with the similarly determined theoretical V_2. Using dimensional analysis, the authors further determined that the density in the farfield region should scale as $(\rho_2/\rho_a)^{1/2}$ where ρ_a is the atmospheric pressure and ρ_2 is determined in a similar manner to D_2 and V_2. Using all of these aforementioned normalizations to define the dimensionless velocity decay rate as $K = \delta(V_2/V)/[(\rho_2/\rho_a)^{1/2}(x/D_2)]$ provides good collapse, as shown in Fig. 2.

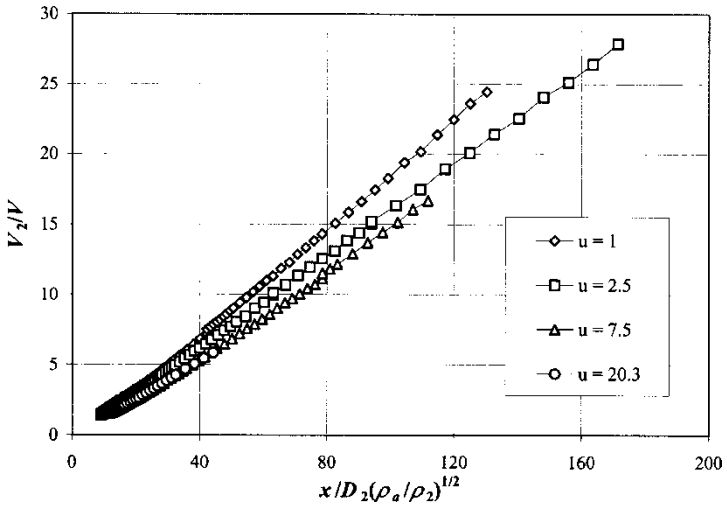

Figure 2. The inverse of the normalized centerline over normalized axial distance is shown for varying pressure ratios, *u*, which correspond directly to the jet Mach numbers. The slope of each line is the dimensionless velocity decay rate, *K*. Taken in whole from Yüceil and Ötügen ("Scaling").

However, there remains a slight effect of decreasing *K* with increasing *Mj*. The authors argue that this is probably due to the effects of compressibility on turbulent mixing, namely the spreading rate of the turbulent shear layer. Earlier work by Papamoschou and Roshko had defined a convective Mach number, M_c, that seemed to affect the turbulent shear layer spreading rates within the range $0.5<M_c<0.9$, where in this range increasing M_c led to decreased turbulent shear layer spreading rates. Thus, where *Mj* corresponds to an M_c within the aforementioned range, in this case for M_j between 1 and 3, which is say all of the cases studied, *K* will decrease with increasing M_j, but for all M_j outside this range, *K* should not experience this effect. As seen in Fig. 3, the difference in *K* between the largest and smallest M_j under study was approximately 18%. The authors argue that the change in *K* due to the effects of compressibility on turbulent mixing is bounded by approximately 20%. The average *K* determined by the authors agrees well with a previous study performed by Zaman, who did not see this same

problem of decreasing K with increasing M_j, although that is best explained by the fact that he was working within a smaller range of M_j, between 1.0 and 1.5.

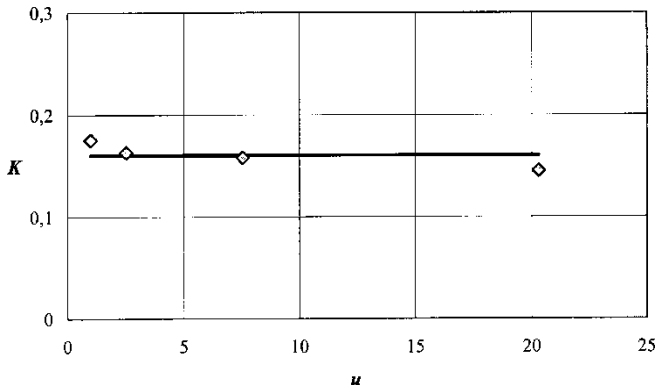

Figure 3. The centerline velocity decay rate K from Figure 2 is plotted here, showing the slight decrease in K as the pressure ratio u, which corresponds to the jet Mach number, increases. Taken in whole from Yüceil and Ötügen ("Scaling").

The authors chose to measure the axial growth rate of the jet using the growth of the velocity half-width, b_v, which is easily used because of the known Gaussian velocity profile. Using similar arguments to those used for the centerline velocity decay rate, the velocity V is normalized with V_2 and the axial distance x is normalized with D_2. This analysis provides very good collapse, as shown in Fig 4.

Further analysis on the temperature field is then performed using much the same methods as for velocity. Because the normalized temperature profile in the farfield jet is self-similar and Gaussian just like the velocity profile, much of the earlier analysis can be easily applied. Assuming that the local temperature is approximately equal to the atmospheric temperature and reasoning that the centerline kinetic energy is equal to the difference in enthalphy between the jet centerline and the ambient, the normalized temperature can be expressed $(T_a\text{-}T)/(T_a\text{-}T_{CL}) = e^{2\ln 2(r/b_T)} = e^{4\ln 2(r/b_v)}$. Thus, not only can b_T be directly related to b_v, but the so can the temperature half-width growth rate be directly

related to the velocity half-width growth rate. This is shown in Fig 5, which shows good collapse.

The authors also attempted to show that, similar to in the velocity case, a universal inverse decay law could be obtained for the centerline temperature in the farfield jet. However, they were unsuccessful in doing so, as shown in Figure 6.

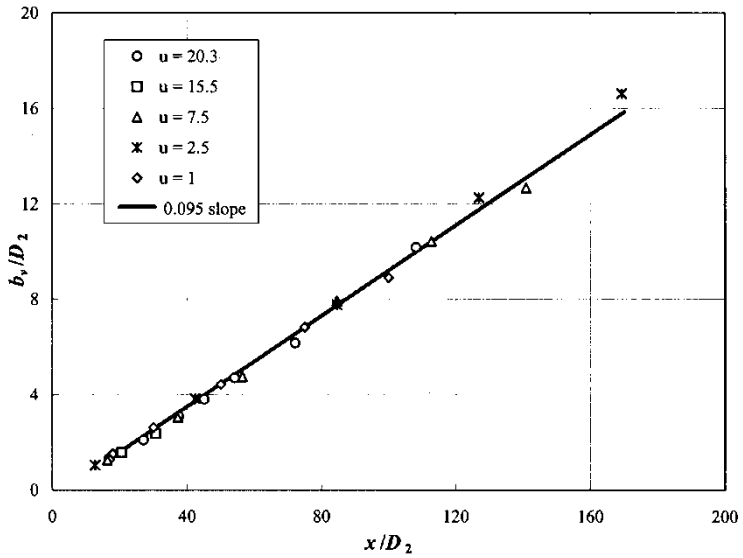

Figure 4. Normalized velocity half-width over normalized axial distance. The slope is the growth rate of the half-width velocity. Taken in whole from Yüceil and Ötügen.

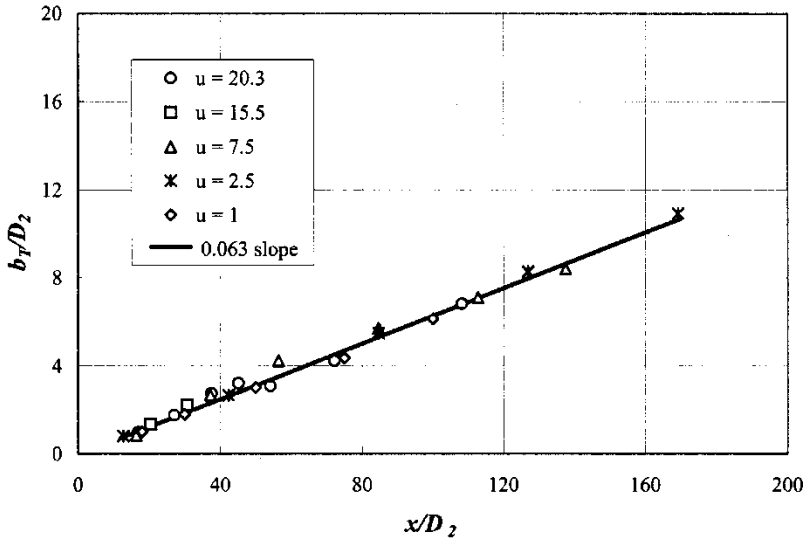

Figure 5. Normalized temperature half-width over normalized axial distance. The slope is the growth rate of the half-width temperature. Taken in whole from Yüceil and Ötügen ("Scaling").

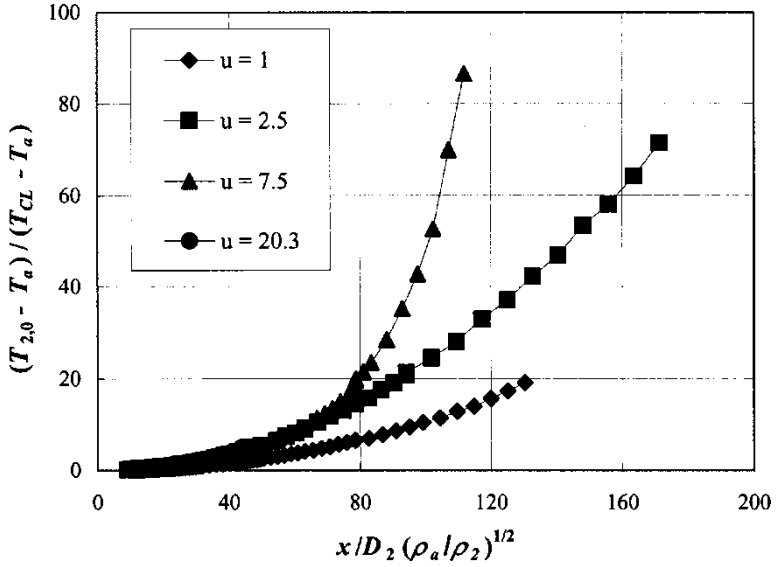

Figure 6. The normalized centerline temperature over the normalized axial distance. Clearly, the attempt to show an inverse decay law was unsuccessful, as the different jets do not approach collapse. Taken in whole from Yüceil and Ötügen ("Scaling").

COMPUTATIONAL BENCHMARKING

In the development of the model, it will be necessary to benchmark the new computational results to those put forward by previous studies of jet flows. The studies under review in this section were chosen for relevance to the PWR LOCA problem and ease of comparison. All of the studies fall under one of two categories—free jet expansion or impinging jets—and so first this report will discuss free jet expansion studies and then will discuss impinging jet studies.

The free jet expansion studies provide some insight into the model development process. Zerkle attempts to correct and explain some deficiencies in the earlier computational studies performed by Teske, Boschitsch and Curbishly at Continuum Dynamics, Inc (CDI). The original CDI study analyzes the case of supersonic free jet expansion into ambient air for both air and high-quality steam. In each case, the flow is assumed to be choked at the nozzle, which has a diameter of 299 mm. For high quality steam, CDI uses NPARC code to calculate the centerline static pressure for three different cases given in Table 1 below. These results are then compared to experimental results for centerline static pressure contained in the CDI report for an experiment where a pressure vessel containing high quality steam blows down through a nozzle of 299 mm. Thus, the three cases in Table 1 correspond to different times during the blowdown of the pressure vessel.

Stagnation Pressure (psia)	637.4	537.0	345.4
Stagnation Temperature (K)	949.0	949.0	949.0
Blowdown time (s)	10	20	50

Table 1. Upstream conditions for the CDI supersonic steam free jet expansion study with centerline static pressure results.

Additional computations are then performed to compare a high-quality steam jet to an air jet with similar Reynolds numbers. To maintain identical Reynolds numbers between the two cases, the stagnation temperature of air is adjusted, though the stagnation pressure remains identical in both cases, as can be seen in Table 2 below. The computations performed give the centerline stagnation pressure.

Stagnation Pressure (psia)	618.4
Air Stagnation Temperature (K)	894.0
Steam Stagnation Temperature (K)	949.0

Table 2. Upstream conditions for the CDI steam and air free jet expansion study with centerline stagnation pressure results.

Zerkle noted some issues with the analysis performed by CDI. First, he argues that CDI uses an incorrect analysis to determine the ratio of specific heats, γ, for high quality steam and so chooses the commonly accepted value of 1.27 for his own analysis. Second, the CDI results cannot explain why the downstream air jet contains regions of high stagnation pressure while the steam jet does not. Thus, Zerkle uses Fluent to analyze the same problem for a few of the cases analyzed in the CDI report. These cases are laid out in Table 3 below. Further, not only do the Zerkle results include the same centerline static and stagnation pressure graphs as in the CDI results, but they also include 2-D static and stagnation pressure contours, and an example is shown in Figure 7.

Fluid	Steam	Air
Stagnation pressure (psia)	637.4	618.4
Stagnation temperature (K)	949.0	894.0

Table 3. Upstream conditions for steam and air free jet expansion in the Zerkle report.

Zerkle's results have some marked differences from the CDI results, most notably the location and stagnation pressure gradient of the shock and the erasure of the unexplained downstream regions of high stagnation pressure in the air jet, as shown in Figure 8. To attempt to explain these differences, Zerkle increases the coarseness of his computational mesh and adjusts the ratio of specific heats to the CDI value of approximately 1.13 to better reflect the CDI case conditions. Although these adjustments do change the location of the shock to be closer to the CDI case, the other differences remain. Zerkle suggests that perhaps the difference can be attributed to the differences between the algorithms in the two codes, NPARC and FLUENT. Whereas NPARC uses a time-march algorithm which solves time dependent terms in the conservation equations, the FLUENT solver computes a steady state solution which solves the conservation equations through control volume analysis in space.

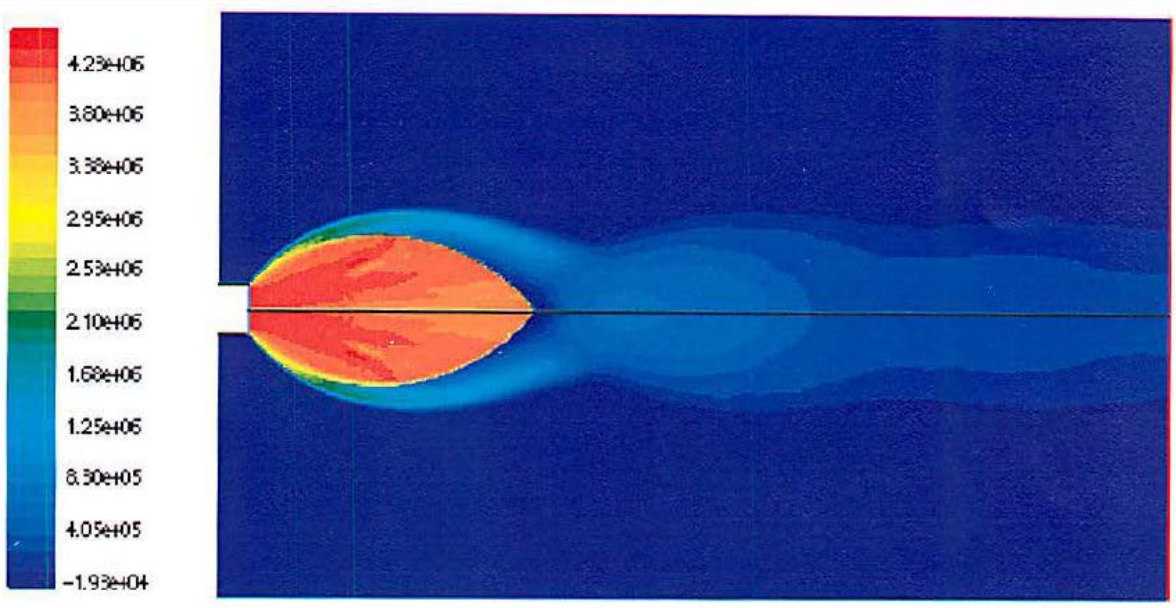

Figure 7. Stagnation pressure contours for steam free jet expansion with upstream stagnation pressure 637.4 psia and upstream stagnation temperature 949 K. Taken from in whole from Zerkle.

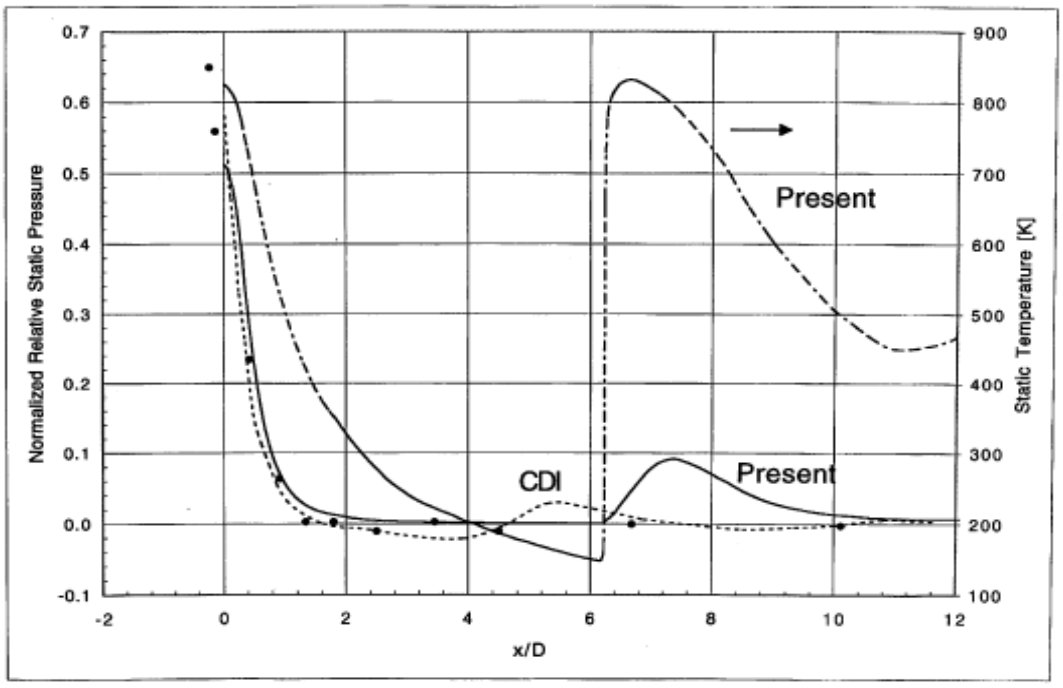

Figure 8. Comparison of normalized relative centerline static pressure for CDI and Zerkle, denoted as "Present." Dashed lines represent air, solid lines represent steam and dots represent experimental data for steam. Taken in whole from Zerkle.

It should be noted that the results from both CDI and Zerkle agree well with the steam jet experimental data from the CDI report, as can be seen in Figure 8. However, this is readily explained when two issues with the experiments are considered. First, the spatial resolution of the experiments is relatively sparse, certainly too sparse to resolve a shock. Secondly, the probe used to measure the static temperature created a physical disturbance in the flow, possibly changing where the shock formed in the flow. Further, uncertainties in the experimental results are not included along with the experimental data, and thus the precision of the experimental data is unknown.

However, the bulk of the studies included in this report are primarily concerned with impinging jets. Weigand et al. present the canonical modeling study of impinging

two-phase jets. The computational model is essentially a modification of Sandia's CSQ code, which uses an Eulerian finite difference method to solve the conservation equations and is thus always marching forward in time. CSQ has since been upgraded to CTH, which is still supported by Sandia. In the model given in Weigand et al., a vessel with constant properties—essentially an infinite reservoir—blows down through a nozzle of fixed diameter that is essentially fixed as a hole in an infinite surface. The jet impinges on an infinite flat surface a fixed distance L away from the nozzle. The HEM critical flow model, which only depends on the stagnation properties of the fluid in the vessel, is used to evaluate the flow from the break. The jet then develops into a conical, supersonic liquid core. Finally, the bulk of the jet forms and eventually equilibrates with ambient pressure in the far field. This final section is where most of the computation is necessarily focused and indeed was so computational intensive at the time that jet behavior in the far field—although present in all modeling considerations—was not accurately modeled due to inadequate resolution.

The model developed in Weigand et al. is used to create several case studies at various upstream conditions jetting to atmospheric conditions. These studies result in density and pressure contours; velocity magnitude, sound speed, temperature and pressure distributions along the radius of the target wall; velocity fields; density, temperature, and static pressure distributions along the centerline. A representative sample of some of these results is given in Figure 9, but the range of conditions studies is given in Table 4.

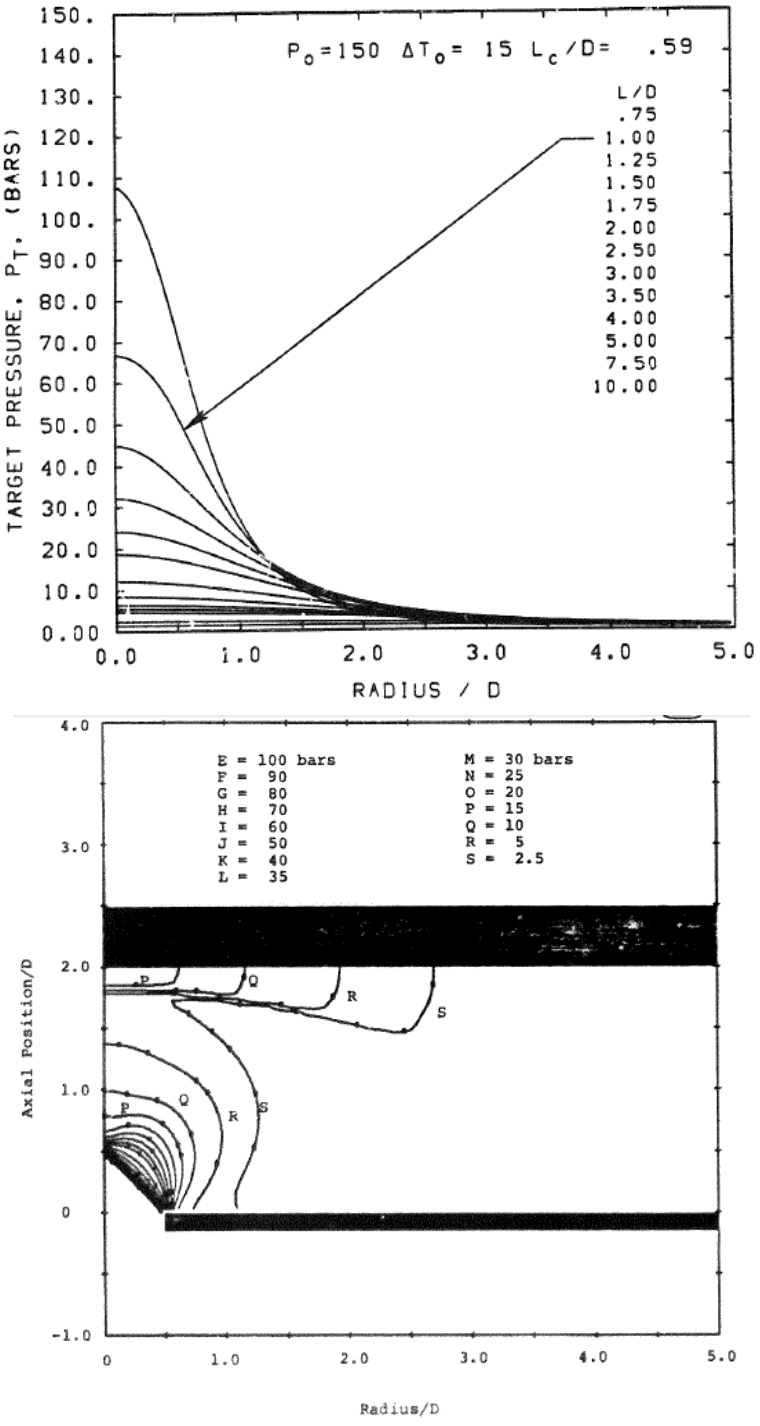

Figure 9. Examples of pressure distribution and pressure contour results from the Weigand model. Taken in whole from Weigand et al.

Upstream subcooling (K)	0, 15, 35, 50, 70
Upstream steam quality	0, 0.01, 0.05, 0.1, 0.2, 0.333, 0.75, 0.99
Upstream stagnation pressure (bars)	60, 80, 100, 130, 150, 170
Normalized target position L/D	0.5, 0.75, 1.0, 1.25, 1.50, 1.75, 2.0, 2.5, 3.0, 4.0, 8.0

Table 4. Test conditions for impingement jet computations in Weigand et al.

Weigand et al. also include an initial comparison with experimental data that shows good agreement for most of the jet, as shown in Figure 10; however, close to the nozzle exit the errors occasionally verge on 25%. It must be noted that because the data included in the report is considered proprietary, the centerline pressure shown is given without units. To address the near-nozzle problem, Kawasaki et al. propose allowing the jet to expand backwards near the jet exit. Thus, their jet does not exit from a hole in an infinite surface, but instead from a pipe exit. Using this method and the same experimental data as in Weigand et al, they were able to decrease the near exit error from approximately 25% to under 10%. They also found that this correction resulted in the jet momentum is also dispersed farther in the radial direction than predicted in Weigand et al. Results are provided in the form of velocity fields, void fraction distribution and target wall pressure distributions, examples of which are given in Figure 11. Test conditions are also shown in Table 5.

Pipe diameter (mm)	500
Normalized target position L/D	1.25, 2.0, 4.0
Upstream stagnation pressure (MPa)	2.23, 2.33, 2.53. 2.46
Upstream void fraction	0.02, 0.3

Table 5. Test conditions for impingement jet computations in Kawasaki et al.

Pipe diameter (mm)	25, 76, 102
Normalized target position L/D	0, 0.1, 0.2, 0.4, 0.6, 1.0, 1.5, 2.0, 2.5, 3.0
Upstream stagnation pressure (Mpa)	0.64, 1.3, 3.4, 6.3, 7
Upstream subcooling (K)	0, 20, 27, 30, 59

Table 6. Test conditions for impinging jet experiments in Forrest et al.

Forrest et al. also give experimental data for impinging two phase jets. The data consists of impingement plate pressures and static pressure at the centerline for a variety of experimental conditions. The exact conditions studied are presented in Table 6 and representative results in Figure 12.

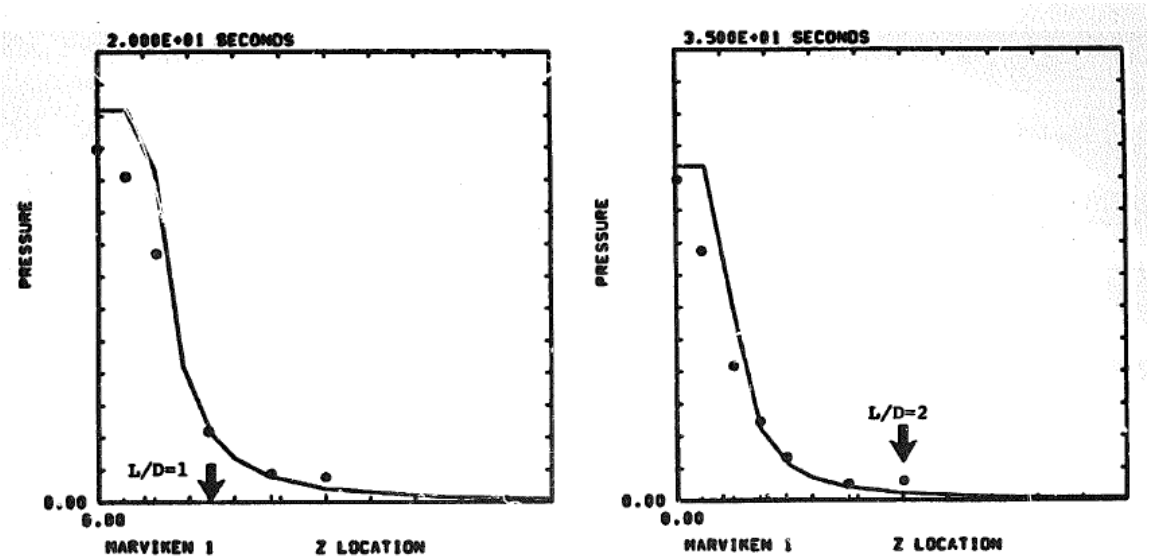

Figure 10. A comparison of the model in Weigand et al. to experimental results, shown without units to preserve proprietary data. Agreement is good except near the nozzle for some cases, as shown in these results. Taken in whole from Weigand et al.

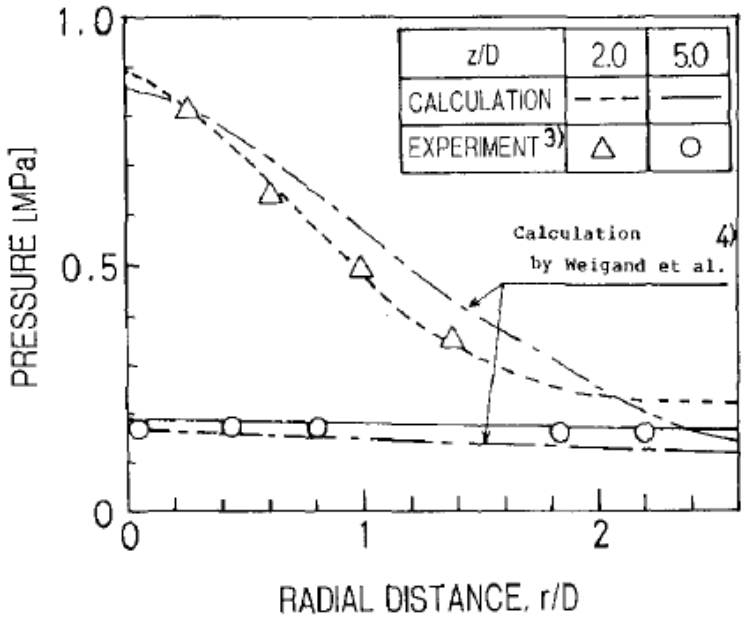

Figure 11. A comparison of the improved model in Kawasaki et al. to the Weigand model with experimental results for additional comparisons. Taken in whole from Kawasaki et al.

Up until this point, all of the cases discussed have benefitted from axisymmetric symmetry. The jet nozzle was always circular and the target under discussion was infinite or at least semi-infinite and thus the problem could be assessed as a two-dimensional problem in cylindrical coordinates. All of the conditions of these studies are given in Table 9. However, because of the possibility that future studies may expand to asymmetric cases, studies of jets from non-circular nozzles and studies of jets impinging on targets other than infinite flat plates have also been gathered.

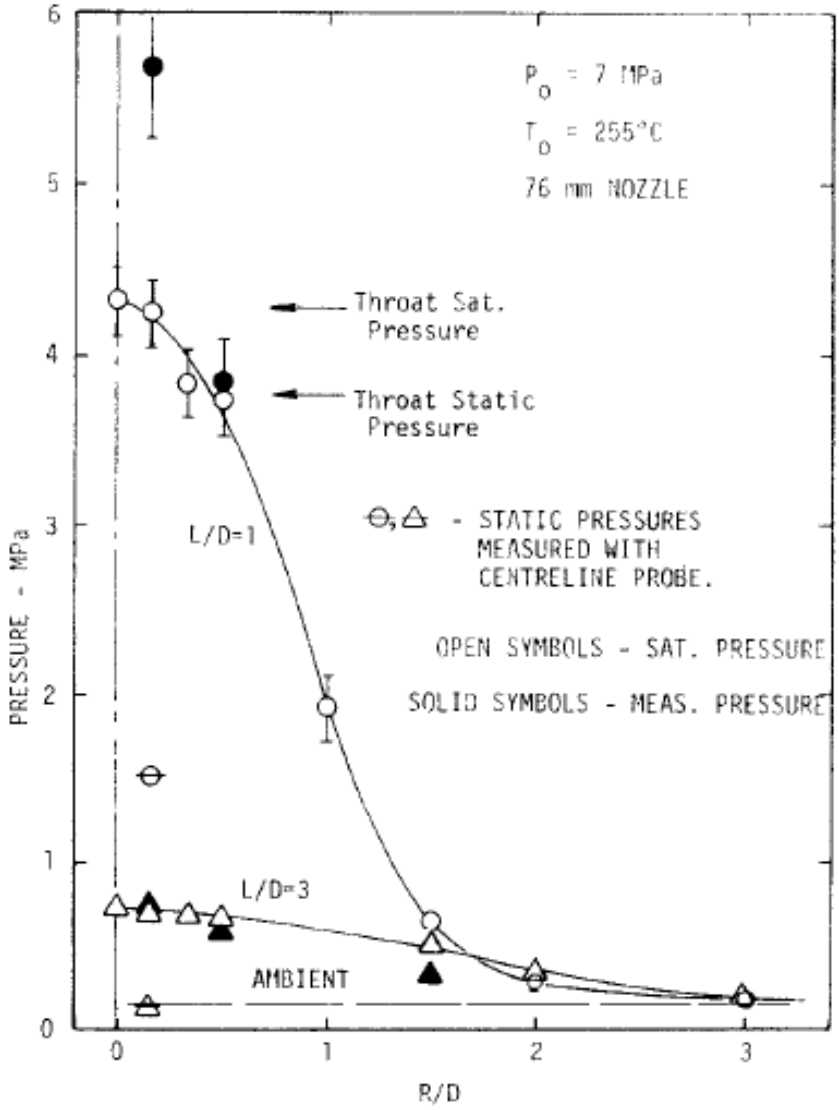

Figure 12. An example of some experimental data for impingement pressure distributions from Forrest et al. Taken in whole from Forrest et al.

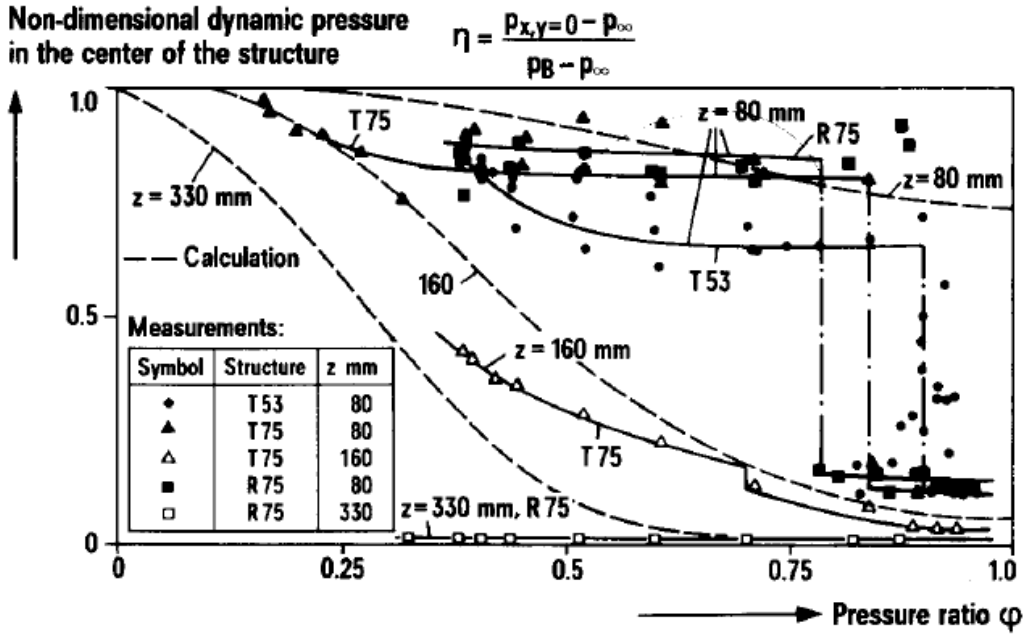

Figure 13. Experimental data from Kastner and Rippel for two-phase jet from a rectangular nozzle impinging on H-beam and pipe targets. Taken in whole from Kastner and Rippel.

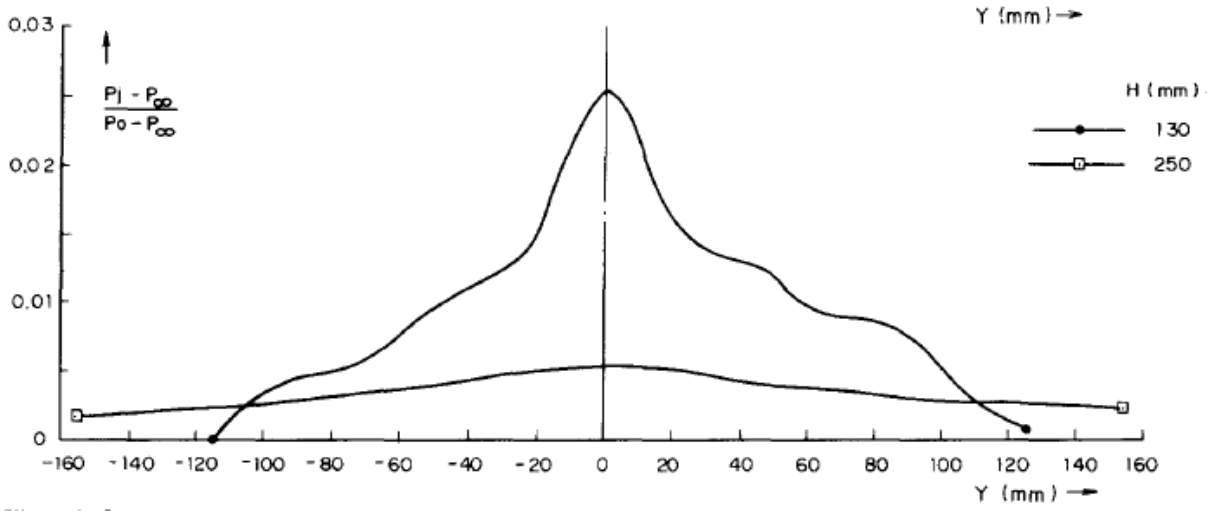

Figure 14. Radial impingement pressure distribution experimental data from Masuda et al. This is only a representative example for this study. Taken from in whole from Masuda et al.

To this end, Kastner and Rippel present results from two-phase water jetting out of rectangular nozzles onto two sizes of h-beams and a pipe. The dimensions of the rectangle—where the length equals the pipe diameter and the area equals one tenth of the pipe cross-section—is based on the 0.1-A break required in licensing calculations for German nuclear power plants The experimental data give results for centerline impingement pressure at the target and total jet impingement force distribution along the face of the target. The study also includes a model for the pressure distribution along the target developed from experimental results for impingement pressures along the edge of the target. The experimental conditions are given in Table 7 and the results are presented in Figure 13.

Pipe diameter (mm)	132
Rectangular nozzle dimensions (mm)	132 x 10.4
H beam target dimensions (mm)	53 x 53, 75 x 75
Pipe target diameter (mm)	75
Upstream stagnation pressure (bars)	77
Target distance from nozzle (mm)	80, 160, 330
Ratio of upstream saturation pressure at stagnation temperature to upstream stagnation pressure	More than 15 values between 0.17 and 0.9

Table 7. Test conditions for rectangular nozzle impinging jet experiments in Kastner and Rippel.

Further, experimental results with jets from elliptical nozzles impinging on flat plates are presented by Masuda et al. This study actually also includes free jet pitot pressure profiles from elliptical nozzles. However, in this case the fluid is always dry saturated steam in the pressure vessel. The test conditions are presented in Table 8 and some representative results given in Figure 14.

Normalized target position L/D (mm)	5, 15, 33, 53, 130, 250
Upstream stagnation pressure (MPa)	4.02, 4.56
Elliptical nozzle axis lengths (mm)	5.0 x 19.7

Table 8. Test conditions for elliptical nozzle impinging jet experiments in Masuda et al.

To pursue these benchmarks, first this report proposes solving the freely expanded jet for air, then steam. Because there are fewer extreme gradients in freely expanded jets, this will ensure that the problems are properly set up before the added numerical complications that come from more extreme gradients. Once both of those benchmarks have been successfully met, then benchmarks for 2-D impinging jets can be performed. Again, this report proposes starting with the simpler case of dry saturated steam before moving on to wet steam and then subcooled liquid. With the subcooled liquid cases, benchmarks should first be performed based on the results in Weigand et al. before exploring backflow to better match with the Kawasaki et al. results and experimental data. After the 2-D impinging jet cases have been benchmarked, then future studies can explore the 3-D cases. These studies should start with the free jet dry steam experiments with jets from elliptical nozzles before adding the complications of impinging jets and multiphase flow.

Fluid	Stagnation Pressure (psia)	Stagnation Temperature (K)	Quality	Target position L/D
Air	618.4	894.0	n/a	Free jet
Superheated steam	637.4	949.0	n/a	Free jet
Superheated steam	537.0	949.0	n/a	Free jet
Superheated steam	345.4	949.0	n/a	Free jet
Superheated steam	618.4	949.0	n/a	Free jet
Saturated water	1160	430	0, 0.01, 0.05, 0.1, 0.2, 0.33, 0.75, 0.99	.5, 0.75, 1.0, 1.50, 2.0, 2.5, 3.0, 4.0, 8.0
Subcooled water	1160	415, 395, 380, 360	n/a	.5, 0.75, 1.0, 1.50, 2.0, 2.5, 3.0, 4.0, 8.0
Saturated water	870	422	0, 0.01, 0.05, 0.1, 0.2, 0.33, 0.75, 0.99	.5, 0.75, 1.0, 1.50, 2.0, 2.5, 3.0, 4.0, 8.0
Subcooled water	870	407, 293, 372, 352	n/a	.5, 0.75, 1.0, 1.50, 2.0, 2.5, 3.0, 4.0, 8.0
Saturated water	1450	499	0, 0.01, 0.05, 0.1, 0.2, 0.33, 0.75, 0.99	.5, 0.75, 1.0, 1.50, 2.0, 2.5, 3.0, 4.0, 8.0
Subcooled water	1450	484, 469, 449, 429	n/a	.5, 0.75, 1.0, 1.50, 2.0, 2.5, 3.0, 4.0, 8.0
Saturated water	1890	506	0, 0.01, 0.05, 0.1, 0.2, 0.33, 0.75, 0.99	.5, 0.75, 1.0, 1.50, 2.0, 2.5, 3.0, 4.0, 8.0
Subcooled water	1890	491, 476, 456, 436	n/a	.5, 0.75, 1.0, 1.50, 2.0, 2.5, 3.0, 4.0, 8.0
Saturated water	2180	510	0, 0.01, 0.05, 0.1, 0.2, 0.33, 0.75, 0.99	.5, 0.75, 1.0, 1.50, 2.0, 2.5, 3.0, 4.0, 8.0
Subcooled water	2180	495, 480, 460, 440	n/a	.5, 0.75, 1.0, 1.50, 2.0, 2.5, 3.0, 4.0, 8.0

Fluid	**Stagnation Pressure (psia)**	**Stagnation Temperature (K)**	**Quality**	**Target position L/D**
Saturated water	2470	513	0, 0.01, 0.05, 0.1, 0.2, 0.33, 0.75, 0.99	.5, 0.75, 1.0, 1.50, 2.0, 2.5, 3.0, 4.0, 8.0
Subcooled water	2470	498, 483, 463, 443	n/a	.5, 0.75, 1.0, 1.50, 2.0, 2.5, 3.0, 4.0, 8.0
Subcooled water	92.8	423, 403, 396, 393, 364	n/a	0, 0.1, 0.2, 0.4, 0.6, 1.0, 1.5, 2.0, 2.5, 3.0
Subcooled water	186	443, 423, 416, 413, 486, 442, 439, 410	n/a	0, 0.1, 0.2, 0.4, 0.6, 1.0, 1.5, 2.0, 2.5, 3.0
Subcooled water	493	469, 449, 442, 439, 410	n/a	0, 0.1, 0.2, 0.4, 0.6, 1.0, 1.5, 2.0, 2.5, 3.0
Subcooled water	914	486, 463, 459, 456, 427	n/a	0, 0.1, 0.2, 0.4, 0.6, 1.0, 1.5, 2.0, 2.5, 3.0
Subcooled water	1020	489, 469, 462, 459, 430	n/a	0, 0.1, 0.2, 0.4, 0.6, 1.0, 1.5, 2.0, 2.5, 3.0

Table 9. All of the conditions for the studies of jets from cylindrical nozzles.

Chapter 3: Model Development

This chapter will go through the proposed methodology for development of the model. The first section focuses on the dimensional analysis of the jet and the development of four new variables related to the damage potential of the jet: the jet thrust coefficient, jet moment coefficient, jet shear coefficient, and jet shear moment coefficient. The second section proposes numerical methods to be used in fitting the model to the data. The third section discusses possible functional forms and methods for determining the best model and reducing uncertainties.

DIMENSIONAL ANALYSIS

This section will explain the use of dimensional analysis in the development of the model. The first subsection will explain some assumptions and detail the use of dimensional analysis to determine the dimensionless parameters necessary to characterize similar jets. The second subsection will exploit the fact that non-dimensionless parameters developed with the Buckingham-π approach to develop new parameters of interest. Specifically, it will show how the addition of the dimensionless axial distance to the group of independent parameters allows for the development of several new parameters of relevant to jet pressure field and the damage potential.

Dimensional Analysis to Characterize Similar Jets

The jet is assumed to be in a pseudo-steady state such that as the fluid is being released to the atmosphere, the stagnation pressure and temperature at the outlet remain the same. In reality, during an extended blowdown the temperature of the steam would increase and the stagnation pressure would decrease. However, these changes in hot leg coolant fluid properties would occur slowly relative to the jet formation, and furthermore the jet's damage potential is greatest under the conservative assumption that steady flow

is maintained upstream of the break. Thus the pseudo-steady state assumption provides conservative results.

As discussed in the previous chapter, the current model divides the jet into three regions: the nearfield, midfield and farfield regions. The underlying analytical technique used in developing the model is dimensional analysis. Dimensional analysis has been used in the previous analyses of the farfield regions and in this paper it is further expanded to describe the nearfield and midfield regions of the jet as well.

Dimensional analysis is powerful for depicting complex, multivariate problems. This study uses a Buckingham-π approach in order to determine the number of relevant dimensionless parameters. This method allows for a systemic understanding of the minimum number of parameters and their dimensionless groupings necessary to relate independent parameters to the dependent flow properties of interest. According to the classical Buckingham-π theorem, the number of relevant dimensionless parameters is equal to the independent parameters that characterize the problem less the number of relevant dimensioned parameters.

This problem involves both mass and heat transfer and thus has four relevant basic dimensions: mass, temperature, time and length. Determining the independent parameters is somewhat more difficult, and must take into account the system geometry, flow conditions, and fluid properties relevant to the jet. This study only considers the case of an axisymmetric circular jet, so there is only one relevant geometric parameter, the diameter of the jet outlet.

Determining the number of independent flow conditions is more complex. Because it is assumed that the flow is choked at the jet outlet, all flow conditions at the jet outlet can be determined with only the initial stagnation pressure and temperature of the fluid using only the isentropic relations for compressible flow, as shown below

$$T_{outlet} = \frac{T_0}{1 + \frac{\gamma - 1}{2}}$$

$$P_{outlet} = \frac{T_0}{\left(1 + \frac{\gamma - 1}{2}\right)^{\frac{\gamma}{\gamma - 1}}}$$

$$v_{outlet} = \sqrt{\gamma R T_{outlet}}$$

where T_{outlet} is the fluid temperature at the outlet, T_0 is the initial stagnation temperature of the fluid, γ is the ratio of specific heats, P_{outlet} is the fluid pressure at the outlet, and v_{outlet} is the velocity of the fluid at the outlet.

This fluid, however, also interacts with the atmosphere, so the atmospheric conditions must also be characterized. Because the atmospheric fluid is assumed to be quiescent air and therefore at stagnation conditions, there are only four independent flow conditions: the initial stagnation pressure and temperature of the fluid at the exit and the pressure and temperature of the atmosphere that the jet flows into.

The last set of independent parameters, the fluid properties, is perhaps the most difficult to determine. Because this study is concerned with both the momentum and heat transfer in the fluid, both the kinematic viscosity v and thermal diffusivity α of the fluid must be known. To properly characterize the fluid, the specific heat at constant pressure C_p and the specific heat at constant volume C_v must also be known. This gives a total of four fluid properties. The total number of independent parameters comes to nine as shown in Table 10, and the number of dimensionless parameters is therefore five.

Three of the five dimensionless parameters that characterize the jet are the same over the entire jet region, while the final two were chosen separately for each of the three jet regions in the model. Over the entire jet region, this study is concerned with both thermal and momentum diffusion over the entire jet region, so the Prandtl number, defined as the ratio of thermal diffusivity to kinematic viscosity, is chosen.

Independent Parameter	**Dimensions**	**Category**
Diameter	[m]	Geometric
Initial stagnation pressure	[Pa]	Flow condition
Initial stagnation temperature	[K]	Flow condition
Atmospheric pressure	[Pa]	Flow condition
Atmospheric temperature	[K]	Flow condition
C_v	[J/kgK]	Fluid property
C_p	[J/kgK]	Fluid property
ν	[m^2/s]	Fluid property
α	[m^2/s]	Fluid property

Table 10. A table of the independent parameters is here provided along with their dimensions and whether they represent relevant geometry, flow conditions or fluid properties.

Nearfield	**Midfield**	**Farfield**
Pr	Pr	Pr
θ_T	θ_T	θ_T
γ	γ	γ
Re	Re	M_j
$*L_{md}$	$*L_{tr}$	$*K$

Table 11. The dimensionless parameters for the jet similarity studies in each of the regions of the jet are shown above. The first four dimensionless parameters in each category can be trivially calculated from upstream conditions. The starred dimensionless parameters are the determined dimensionless parameters which must be determined by an equation relating it to the other dimensionless parameters.

To easily characterize the jet, the Prandtl number is calculated at the fluid conditions upstream of the break. The model will also be affected by the thermal properties of the jet fluid, since both steam and air are under study, and the ratio of specific heats is chosen to account for this. Because of the ratio of specific heats is important for calculating other choked flow conditions at the breakpoint, the ratio of specific heats should be evaluated for the breakplane's choked flow conditions. Finally, the magnitude of the temperature difference between the jet and the atmosphere is accounted for in the normalized temperature difference θ_T, defined below

$$\theta_T = \frac{T_{0,upstream} - T_{0,atm}}{T_{0,upstream}}$$

where $T_{0,upstream}$ is the stagnation temperature of the upstream fluid, and $T_{0,atm}$ is the temperature of the atmosphere.

For the nearfield jet region modeling, which is based on classical shock dynamics, one dimensionless parameter of interest is the normalized Mach disk location, defined below

$$L_{md} = \frac{X_{md}}{D}$$

where X_{md} is the axial location of the Mach disk and D is the diameter of the jet at the breakplane.

This choice of parameter is based on previous studies as described in Chapter 2. Also, it should be emphasized that because those previous studies have shown the Mach disk location to be a dependent parameter, it is not considered an independent parameter in this analysis (Ashkenas and Sherman). This parameter provides a solid understanding of the initial geometry and expansion of the jet. Because of the effects of turbulence on entrainment between the jet and the atmosphere, the Reynolds number of the jet at the

breakplane is chosen as the final dimensionless velocity parameter. The normalized location of the Mach disk is the only parameter that cannot be trivially calculated with knowledge of the upstream conditions.

Moving into the midfield region, the primary concerns of the model are in determining for how long the midfield transitional region between the nearfield jet region and the farfield jet region persists. Thus the final dimensionless parameter for the midfield is chosen to be what will be called the normalized transition length, which describes the length of the transition region between the nearfield and farfield regions, which corresponds to the midfield, and which is defined as

$$L_t = \frac{X_t}{D}$$

where X_t is the axial location of where the farfield region begins and D is the diameter of the jet at the breakplane.

Also, it should be again emphasized that because those previous studies have shown the location were the farfield region begins to be a dependent parameter, it is not considered an independent parameter in this analysis (Yüceil and Ötügen). Also, because turbulent effects are again a main mode of diffusion in this region, the Reynolds number is chosen as the dimensionless velocity parameter. For ease of comparison, in this region the Reynolds number is still calculated at the breakplane conditions. Again, it should be noted that there is only one parameter that cannot be trivially calculated with knowledge of the upstream conditions: the normalized transition length.

In the farfield region, choice of the final two dimensionless parameters is guided by previous modeling work by Yüceil and Ötügen. Thus, the two parameters for the farfield region are the jet Mach number M_j and the decay parameter K as defined below

$$M_j = [(\frac{p_t}{p_a}^{(\gamma-1)/\gamma} - 1)(\frac{2}{\gamma - 1})]^{1/2}$$

$$K = \frac{d(\frac{V}{V_{exit}})}{d(\frac{x}{D} * \frac{p_a^{\frac{1}{2}}}{p_t})}$$

where p_t is the upstream stagnation pressure of the fluid, p_a is the atmospheric pressure, γ is the ratio of specific heats, V is the centerline velocity, V_{exit} is the velocity at the break plane, and D is the diameter of the break.

Thus, the jet Mach number is a dimensionless velocity parameter determined by the upstream conditions while the decay parameter quantifies the decay rate of the velocity of the jet. Here it should be noted that the decay parameter is the last parameter that cannot be trivially calculated with knowledge of the upstream conditions. For a complete list of all of the dimensionless parameters, please see Table 11 above.

In order to appreciably demonstrate the proper qualification of the jet with the above chosen dimensionless parameters, the data chosen should sweep through an appreciable range of each of the dimensionless parameters. However, this study in particular focuses on the real world problem encountered in nuclear power plants: a fluid with a given stagnation pressure and temperature is released into the atmosphere as a compressible, under-expanded jet. Thus, this study focuses on jets with high stagnation temperatures and pressures similar to that in the hot leg of a boiling water reactor, where the stagnation temperatures and pressures range from approximately 625 to 949 K and 345 to 1000 psi, respectively (Mehta and Pappone). These parameters allow for ranges in the dimensionless parameters as provided in Table 12.

Parameter	Low	High
Θ_T	0.52	0.68
γ	1.2	1.5
Re	60000	2000000
M_j	2.1	3.1

Table 12. The range of dimensionless parameters based on hot leg boiling water reactor conditions is shown to demonstrate the magnitude of the dimensionless parameter sweep that is possible.

In the end, the dimensional analysis performed in this subsection allows the dimensionless parameters that can all be calculated from the initial conditions of the jet to a single new dimensionless parameter. This new dimensionless parameter, from here on referred to as the determined dimensionless parameter, varies for the nearfield, midfield, and farfield. Respectively, the determined dimensionless parameter for each is the normalized Mach disk location, the normalized transition distance, and the decay parameter. However, classifying similar jets is not the focus of this study, which endeavors to gain a better understanding of the damage potential of a given jet in space along its axis.

Expanding Dimensional Analysis to Develop Damage Potential Parameters

In order to further develop the dimensional analysis, a new geometric parameter must be added to this study: x, defined as the distance along the x-axis. Again following the Buckingham-π method, this means there must be an additional dimensionless parameter of interest to the equation. Here it should be emphasized that the dimensionless parameters are not necessarily unique. This study takes advantage of this fact and in fact performs the analysis for several dimensionless parameters that can help gain insight on

the damage potential of the jet. Thus, for each new damage potential parameter, its value along the length can be computed with its own equation relating it to the other dimensionless parameters outlined in the previous subsection.

Now the dimensionless parameters that will prove most helpful in understanding the damage potential of the jet will be chosen. Much of the concern in developing these parameters lay in appropriately reducing the complexity of the jet. At these high temperatures and pressures, the jet is compressible and thus even small changes to the starting conditions of the jet can have relatively large effects on size and shape of the jet due to varying locations of the shock structures. These shock structures mark where large variations in the jet parameters occur, but are not of particular interest.

Studies of similar jets in pressurized water reactors (PWRs) have focused on stagnation pressures in the jet field as a correlate to the damage potential of the jet (Zerkle). The stagnation pressure is an idealized impingement pressure, as if the fluid were brought to a stop isentropically at the impinged surface. Additionally, in many studies this parameter is further limited to the stagnation pressure along the centerline, which allows for direct comparison with previous experimental studies (Zerkle). Thus, the stagnation pressure field provides an easily calculated, though arguably overly conservative, estimate of the impingement pressure.

This study proposes not only a non-dimensionalized stagnation pressure along the centerline, but also four new variables of interest: the jet thrust coefficient, jet thrust moment coefficient, jet shear coefficient, and jet shear moment coefficient, which are defined below in Table 13. Profiles of these variables of interest provide a more thorough understanding of how the stagnation pressure profile changes over both radially and axially over the entire jet field.

Jet thrust coefficient	$\frac{\int_{r=0}^{r=R_{jet}} 2\pi r p_{stag}(r) dr}{p_t D^2}$
Jet thrust moment coefficient	$\frac{\int_{r=0}^{r=R_{jet}} 2\pi r^2 p_{stag}(r) dr}{p_t D^3}$
Jet shear coefficient	$\frac{\int_{r=0}^{r=R_{jet}} 2\pi r \tau(r) dr}{p_t D^2}$
Jet shear moment coefficient	$\frac{\int_{r=0}^{r=R_{jet}} 2\pi r^2 \tau(r) dr}{p_t D^3}$
Centerline pressure coefficient	$\frac{p_{stag}(r=0)}{p_t}$

Table 13. The suggested dimensionless parameters related to damage potential are given above with their definitions. All would be functions of the non-dimensionalized axial distance, *x/D*. The relevant variables are *r*, the radius; R_{jet}, the jet radius at the given *x/D*; p_{stag}, the local stagnation pressure; p_t, the initial stagnation pressure; τ, the local shear; and *D*, the diameter of the jet at the breakplane.

The jet thrust coefficient is calculated by integrating the local stagnation pressure or shear over the radial plane of the jet at a given location on the x axis, and thus provides a measure of the magnitude of the axial momentum of the jet while the jet thrust moment coefficient gives an idea of how the thrust is spread radially over the jet diameter. The addition of the jet shear coefficients allows for some insight into how the jet might damage materials that are weak to shear forces, and may provide insight into whether or not further studies into this phenomenon are necessary. The maximum and minimum jet thrusts and jet shears may also be calculated.

Both the jet velocity and the jet velocity profile change as the jet moves along the x-axis, and so the study proposes defining the jet diameter such that the edges of the jet occur where the velocity is equal to some small percent of the maximum jet velocity along the radius, perhaps 1 percent.

REGRESSION AND NUMERICAL METHODS

One major focus of the model development will be to determine the correct functional form of the equation relating the variables of interest to the non-dimensional parameters. Although technically the function could take any form, the following suggestions contain some of the more likely forms based on knowledge of the problem.

In these suggestions, the variable of interest will be represented with *X* and will show that equations for any of the four (the jet thrust coefficient, jet moment coefficient, and jet shear coefficient, and jet shear moment coefficient) could be represented with the suggested functional form. To further simplify, although the three regions have different associated nondimensional parameters, each of the regions has six total nondimensional parameters which will be represented as Y_n where *n* goes from 1 to 6.

Arguably the simplest possible functional form is similar to that found in relations between the local Nusselt number and the Reynolds and Prandtl numbers in flow over a flat plate:

$$X = C\prod_{n=1}^{6}({Y_n}^{\alpha_n}) + D.$$

where *X* is the variable of interest, each *Y* is a nondimensional parameter, and C, D, and each α are constants. This functional form requires that 8 constants be determined by fitting to the data: *C, D,* and the six α_n.

Another possible functional form that is more complex would include polynomials for any number of the nondimensional parameters:

$$X = \prod_{n=1}^{6}\left[\sum_{N=1}^{x}(C_{n.N}{Y_n}^{\alpha_{n,N}})\right] + D.$$

which can clearly quickly add to the number of constants to be determined.

Of course, the terms can also be added to each other instead of—or in addition to—multiplication:

$$X = \sum_{n=1}^{6} (C_n {Y_n}^{\alpha_n}) + D$$

The real complication comes from when the function includes many of these possibilities, as in the Gnielinski Correlation for forced convection in turbulent pipe flow:

$$Nu_D = \frac{\left(\frac{f}{8}\right)(Re_D - 1000)Pr}{1 + 12.7\left(\frac{f}{8}\right)^{\frac{1}{2}}(Pr^{\frac{2}{3}} - 1)}$$

where

$$f = (0.79\ln(Re_D) - 1.64)^{-2}.$$

In order to prevent time and resources wasted on testing infinite permutations of possible functional forms, some analysis of the problem and of the data should be performed in order to determine some of the more likely functional forms. For example, as discussed in Chapter 2, a previous study showed that *K* is inversely proportional to *x*/*D* in a similar jet (Yüceil and Ötügen). Most insight, however, will probably come from examining and analyzing data from the computational simulations.

The easiest way to gain insight on the functional forms is to analyze the more simple cases first. Thus, analysis should begin where only one non-dimensional parameter changes relative to the variable of interest. After this has been done for all six independent non-dimensional parameters, then the overall best fitting functional form can be inferred more easily. The suggested checks in the next subsection of this chapter will provide some guidance as to whether or not the overall equation has been properly modeled, whether additional relationships have been missed, and how to gather additional data if necessary.

Additionally, many software packages exist that can perform nonlinear least-squares regression to determine the coefficients given a functional form (Seber 662-664).

Thus, possible forms can be tested relatively quickly and easily across the data. However, many of these packages are iterative and require an initial guess for the coefficients. A bad initial guess can give bad or very slow results, and thus some caution and care should be used in choosing initial guesses and in monitoring the iterations of the solver (Seber 665-666).

Once initial guesses have been determined both for the coefficients and the functional form of the solution, the solver should give both the determined coefficients and the residual, R^2, which is a measure of the error in the fit. It is calculated from measuring the difference between the model value and data point for each data point, e_i, as shown below

$$R^2 = \sum {e_i}^2.$$

Thus, a lower residual is associated with a better curve fit. Comparisons of the residuals should be used in determining which functional form of the solution is best.

The size of the residual can also be used to determine the approximated uncertainty for the model. The errors are assumed to be uncorrelated and the independent parameters are assumed to be errorless. Further assuming a Gaussian distribution in error and a constant variance in the error, the variance is given by the formula below

$$\sigma^2 = \frac{R^2}{N - DOF}$$

where N is the number of data points, σ is the mean square error, and DOF is the number of degrees of freedom in the determined equation.

The covariance can then be determined by matrix multiplying the inverse of the transpose of the Jacobian matrix of the parameters by the Jacobian of the parameters

$$covariance = \ (J^T J)^{1/2},$$

where *J* represents the Jacobian, defined as the matrix of the first partial derivatives of the function with respect to each parameter. The variance is then multiplied by the covariance matrix to determine the approximate errors for each of the fit parameters. These computations are commonly performed in the software packages mentioned above, and rely on matrix manipulation techniques like QR decomposition with pivoting.

Given the errors for each of the fit parameters, error bars can then be calculated and graphed over the independent parameter space. These error bars can be used to determine whether or not the model is sufficiently precise or whether more data should be used. If it is determined that more data should be prepared to feed into the model fitting program, analysis should be performed to determine which independent parameter, if any, has the largest influence on the uncertainty. This analysis can be as simple as performing partial derivatives on the fitted analytical equation with respect to each of the independent parameter to perform sensitivity analysis. Another option is to add a few cases that alter only one independent parameter at a time and comparing each new set to see which reflects the greatest reduction in uncertainty. With this option, special care should be taken to ensure that there are no outliers in the set of new data, and that the parameter space is still sufficiently represented with an even spread of data points.

As for an initial estimate of how many data points are necessary to perform this analysis, it must be noted that there are some special factors to consider in this problem. In general, the limiting factor in data acquisition is the time involved in generating the CFD solution for each individual set of upstream conditions and outlet geometry. Each solution will contain hundreds or thousands of data points along the axis of the jet. Because there will be orders of magnitude more data points where the dimensionless distance parameter *x/D* is the only parameter changing, this report assumes that it can be neglected in considerations of the minimum number of necessary data points.

Additionally, because the model is nonlinear, there is no sure way to determine the necessary amount of data for a given desired accuracy. There are, however, some guiding estimations that can be performed, like that of Good and Hardin (211), shown below

$$N = m^n$$

where *N* is the number of data points, *m* is the number of data points needed to fit the equation to the desired precision for a model of only one of the variables, and *n* is the number of independent parameters. Here this report will point out that in the case of this problem, *n* will represent the number of independent parameters less one—the dimensionless axial distance.

Again more assumptions must be made that could be better clarified after data has been generated and analyzed. The number of data points needed to fit the equation to the desired precision for a model of only one of the variables, *m*, is of course unknown in this case. The other variable, *n*, is given as 5, as explained in the previous paragraph. Table 14 shows how the necessary number of data points *N* quickly increases with increasing values of *m* in this case where the number of independent parameters *n* is always equal to 5.

From examining Table 14, it seems like a reasonable number of data points to generate to determine initial uncertainty could be between 10^3 and 10^4. If the function is very complicated however, it is possible that more data points would need to be generated. However, it should be noted that this estimate assumes that each of the independent parameters would require the same number of data points to maintain the desired precision if modeled individually, which is of course untrue. Thus it is possible that if most of the uncertainty is caused by only a few or even only one parameter, the

increase in data points necessary to achieve a desired accuracy would not rise quite as quickly as shown in Table 14.

m	N
3	243
4	1024
5	3125
6	7776
7	16807
8	32768
9	59049
10	100000
20	3200000
100	10^{10}

Table 14. A demonstration of the increasing number of necessary data points *N* with increasing *m*.

CHECKING FOR ERRORS AND ADDRESSING POSSIBLE PROBLEMS

In the previous subsection, the final result of the regression analysis is shown to be a suite of correlations that will allow for a given parameter of interest to be calculated at any point along the length of the jet given only knowledge of the initial stagnation conditions, jet diameter, and fluid properties.

Because of the changing dominant physical processes in the nearfield, midfield, and farfield regimes, each of these regions should have their own fitted curve, and it has been assumed in this analysis that the resulting piece-wise function need not be smooth.

If it is determined that it is important for all of the curves to join in a smooth, piece-wise function, it is possible that an interpolation scheme may be used to meet this requirement.

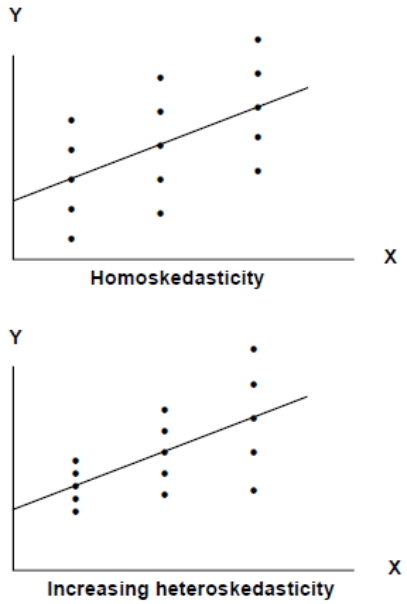

Figure 15. The phenomena of homoskedasticity and heteroskedasticity are shown above. Taken in whole from *Lecture/Discussion*.

If the calculated residuals are normally distributed about zero, the model can be claimed as unbiased, and therefore not missing important independent and explanatory variables. However, if a pattern or trend in the residuals can be detected—if the residuals are not randomly distributed across a chosen variable—then there must be a functional dependence on the variable that has not been accounted for properly in the fitted function itself. If a trend exists, the residuals are said to be heteroskedastic; if no apparent trend exists and the residuals appear to be randomly distributed, the results are said to be homoskedastic. These phenomena are illustrated in Figure 15 above.

Thus, for this problem there are several sets of residual-variable pairs that must be checked for proper homoskedasticity. First, the residuals for the determined

dimensionless parameter for each test case must be plotted against each of the other dimensionless parameters to ensure that there is no heteroskedasticity. The determined dimensionless parameter must be the first to be tested because it will then be used for subsequent correlations for the variables of interest. Similar tests must then be performed for the subsequent correlations; thus, at each individual test case, the residuals for the fitted curve at each data point along the length of the jet must be checked against the normalized distance along the length of the jet. Then for each test case the total sum of the squared residuals along the length of the jet will be calculated. These test case total residuals will then be checked against each of the dimensionless parameters for proper homoscedasticity.

A proposed method to determine whether or not heteroskedasticity is present will be to divide the data each residual-variable pair into several bins over the variable range. The average and standard deviation for each bin will be computed and compared to the average and standard deviation for all of the data. If these differ by some non-trivial amount, the results should be considered heteroskedastic and examined further.

The final problem to check for is the problem of over-fitting the data. Generally, for a given data set, higher order functions will have lower total residuals. Thus, the method of least squares preferentially favors higher-order functions. However, not only can the functions become exceedingly complicated for relatively small changes in accuracy of the model, but higher order functions also bear the risk of over-fitting. Over-fitting is the phenomenon where, essentially, the fitted function ceases describing the physics of the problem under study, and begins to incorporate noise inherent to the specific data set used to determine the fitted function.

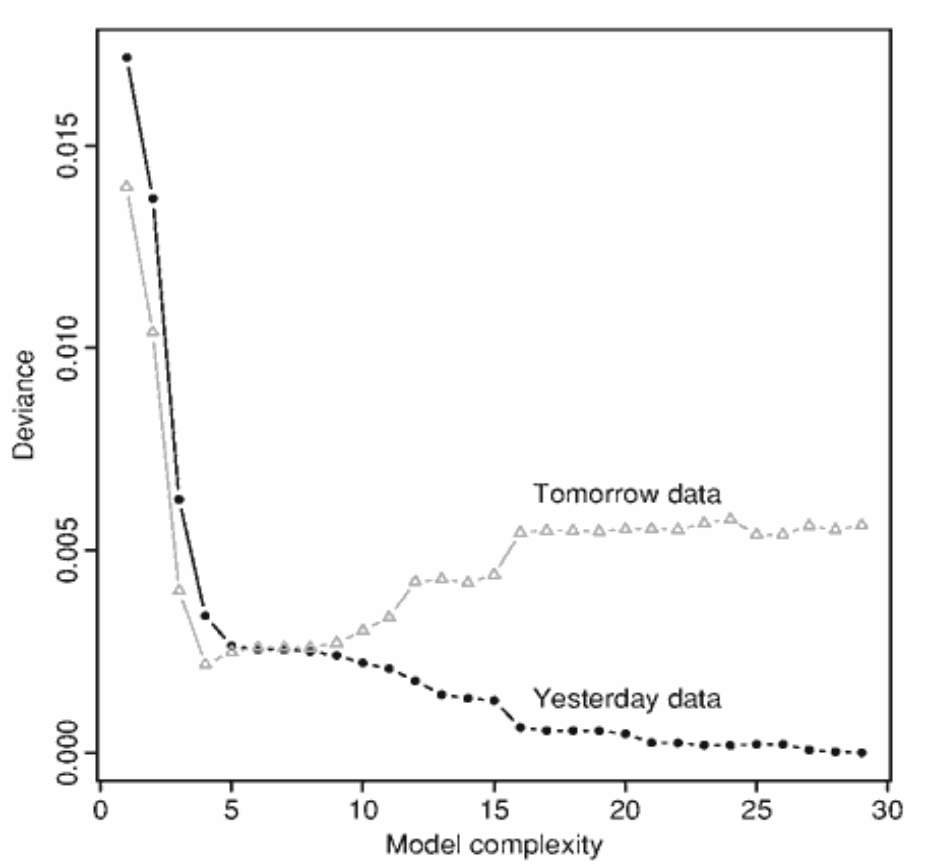

Figure 16. The effects of over-fitting are shown here with a training case labeled "Yesterday data" and a test case labeled "Tomorrow data." Above a model complexity of 4, the test case sees an increase in residuals while the yesterday continues to see a decrease. Thus, above a model complexity of 4, the data is overfitted. Taken in whole from Azzalini and Scarpa (53).

To prevent against over-fitting, the common solution is to divide sample data randomly into different subsets. The first set will serve as a training set which will be used to determine the fitted functions in increasingly higher order. The second set, called the test set, will then be tested against the various fitted functions obtained with the training set. Where over-fitting has occurred, the deviance in the test set cases will begin to increase with the higher order fitted functions even as the residuals in the training set cases, as shown in Figure 16. The simple train-and-test method is used to prevent against

over-fitting in this study. The percentage of data commonly used for training the fitted function can range from as little as 25% to as much as 90% of the total data. In this case, Azzalini and Scarpa recommend using 50% of the data for training (53-54). Because the initial conditions used to generate each test case will be chosen randomly, the test cases will be divided chronologically such that the first half of the test cases are used as the training set and the second half of the test cases are used as the test set.

In the case that the desired multi-dimensional function is highly complex, the analyst may desire to see data with one or more of the dimensionless parameters fixed while sweeping through the others. For some dimensionless parameters this will be trivial. For example, maintaining the normalized temperature difference θ_T while changing other parameters only requires that the stagnation temperatures of the upstream fluid and atmosphere remain steady; changing the upstream stagnation pressure could then be used to change other parameters like the Reynolds number and obtain more data. However, some of the other cases are more complicated, like the pair of θ_T and the ratio of specific heats γ, which both change with the stagnation temperature of the upstream fluid.

When necessary, these data points may be simulated with the method of local data regression. This method uses the data points near to the desired data point to determine the value of the desired data point. This method scales well multi-dimensionally, but the following will describe a two-dimensional analysis for ease of explanation. Essentially, this method determines the unknown value of y_i at a given x_i using known values of y and known values of x.

Functionally, this is expressed as

$$\min_{\beta_0,\beta_1} \sum_{i=1}^{n} \{y_i - \beta_0 - \beta_1(x_i - x_0)\}^2 w_i$$

where w_i is a weighting function and β_0 and β_1 are constants. A common weighting function is given as

$$w_i = \frac{1}{h} w\left(\frac{x_i - x_0}{h}\right).$$

While it has been proven extensively that the choice of the weighting function *w* has little effect, the choice of *h* can have a large effect (Azzalini and Scarpa 72). This study recommends the weighting function above for its simplicity. As for the choice of *h*, although there exist rigorous means of determining *h*, graphical determination is usually simpler and more effective (Azzalini and Scarpa 73), and thus is the method recommended to determine *h* in the cases where local data regression is necessary.

Chapter 4: Conclusion

This report has proposed a methodology for developing a model of a compressible steam jet that allows for an end user to easily predict the damage potential of the jet. To this end, this report also developed and defined four new variables related to the damage potential of the jet: the jet thrust coefficient, jet moment coefficient, jet shear coefficient, and jet shear moment coefficient.

Using computational fluid dynamics simulations as a source of data instead of using experiments allows for measurements to be extracted for thousands of points in space, which is part of the reason that this report could develop the integral-based damage potential coefficients listed above. While these coefficients could be verified experimentally in future studies, it would be difficult to accumulate the amount of data necessary to accurately determine fit coefficients using only experiments.

The model provides a way to simplify the vast amounts of data contained in computational fluid dynamics simulations, using analysis of the fluid dynamics and thermodynamics of the jet to structure the model. Much of the analysis is devoted to understanding the important characteristics of different regions of the jet, drawing on previous studies which tended to only focus on a single region of the jet without relating it to the jet as a whole. The non-dimensional analysis method used to structure the model to characterize the entire jet is the main thrust of this report, as it allows for insight into the jet dynamics using only the upstream conditions of the jet.

This report also provides the best data fitting methodology for determining the fit coefficients of the model. This methodology includes checking for common modeling errors like heteroskedasticity and overfitting, how the data used to determine the fit coefficients should be generated randomly in the parameter space and then divided into a

training set and a test set, and how data points can be simulated with data regression techniques when necessary. These techniques were chosen to best suit the nature of the problem and the resultant model.

Additionally, this report proposes methods for determining the correct functional form of the guiding equations to determine the parameters of interest. Several functional forms are proposed, along with discussion of analytical and computational methods to choose the best functional form. Lastly, methods for determining uncertainty in the fit parameters and guidance on the determination of the necessary number of data points are provided.

Future studies could use the methodology proposed in this report to develop the model, determine coefficients and compare the results from the resultant equations to results from live experiments. This methodology could also be further expanded to allow for multiphase jets where pressurized water is jetted to atmosphere, resulting in a compressible jet with water in both the liquid and vapor phases. This would be the course of action necessary to develop a model for LOCA's in pressurized water reactors.

In short, the model developed with this methodology has many advantages over previous models in that it is easily calculated with knowledge readily available to plant operators and it provides new metrics that allow for a quick and intuitive understanding of the damage potential of the jet.

References

Abramovich, G.N. *The Theory of Turbulent Jets.* Cambridge, MA: MIT Press 1963.

"ANSYS FLUENT 12.0 Theory Guide." Web. 1 Dec. 2011. <http://my.fit.edu/itresources/manuals/fluent/>

Ashkenas, Harry, and Frederick S. Sherman. "The structure and utilization of supersonic free jets in low density wind tunnels (Inviscid and viscous flow in central core of supersonic free jet in wind tunnel, noting shock wave location at high Reynolds number)." *RAREFIED GAS DYNAMICS, PROCEEDINGS OF THE TORONTO, CANADA* (1966): 84-105. Print.

Azzalini, Adelchi, and Bruno Scarpa. *Data Analysis and Data Mining : An Introduction.* Oxford: Oxford University Press, USA, 2012. Print.

Bogdanoff, D. W. "Compressibility effects in turbulent shear layers." *AIAA journal* 21.6 (1983). Print.

Forrest, C.F., K.S. Shin, W.I. Midvidy, R.E. Pauls, and N. Wahba. "Measurements of impact loads and expansion of flashing water jets." *Nuclear Engineering and Design*. Vol. 99. 1 Feb. 1987: 53-61. Print.

Good, P.I., and J.W. Hardin. *Common Errors in Statistics (And How to Avoid Them)* 3rd ed. Hoboken, New Jersey: Wiley 2009.

Groppengiesser, H. "Study on the stability of boundary layers and compressible fluids, TT F-12786." A study prepared at NASA. 1970.

Gutmark, E. J., K. C. Schadow, and K. H. Yu. "Mixing enhancement in supersonic free shear flows." *Annual Review of Fluid Mechanics* 27.1 (1995): 375-417. Print.

Kastner, W., and R. Rippel, "Jet impingement forces on structures — Experiments and empirical calculation methods." *Nuclear Engineering and Design*. Vol. 105. Issue 3. 2 Jan. 1988: 269-284. Print.

Kawasaki, Terufumi, Masanori Naitoh, and Takashi Kamo. "Numerical and experimental study of two-phase jet impingement." *Nuclear Engineering and Design*. Vol. 99. 1 Feb. 1987: 15-23. Print.

Lecture/Discussion: Weighted Least Squares. Berkeley, CA. *University of California, Berkeley Economics*. 22 Mar. 1999. Web. 7 Aug. 2012.

Masuda, F., T. Nakatogawa, K. Kawanishi, and M. Isono. “Experimental study on an impingement high-pressure steam jet.” *Nuclear Engineering and Design.* Vol. 67. Issue 2. Jan 1982: 273-286. Print.

Mehta, Haryadal S., and Daniel C. Pappone. "New Generations of BWRs." *Companion Guide to the ASME Boiler and Pressure Vessel Code*. 3rd ed. Vol. 3. New York, NY: ASME, 2009. Print.

Papamoschou, Dimitri, and Anatol Roshko. "The compressible turbulent shear layer: an experimental study." *Journal of Fluid Mechanics* 197.1 (1988): 453-477. Print.

Seber, George AF, and Christopher John Wild. *Nonlinear regression*. Vol. 503. Wiley-Interscience, 2003. Print.

Soetrisno, M., D.S. Eberhardt, J.A. Greenough, and J.J. Riley JJ. “Confined compressible mixing layers.”*AIAA Paper 88-3676* (1990). Print

Teske, M. E., A.H. Boschitsch, and T.B. Curbishly. "Zone of Influence as Defined by Computational Fluid Dynamics, C.D.I. Report No. 96-0 l.” *Utility Resolution Guide for ECCS Suction Strainer Blockage, Vol 3, NED0-32686-A*. Print.

Weigand, G.G., et al. “NUREG/CR-2913, SAND82-1935.” A study prepared at Sandia National Laboratories. 1983. Print.

Young, Wen S. “Derivation of the free-jet Mach-disk location using the entropy-balance principle.” *Physics of Fluids* 18.11 (1975): 1421-1426. Print.

Yüceil, K. Bülent, and M. Volkan Ötügen. "Scaling parameters for underexpanded supersonic jets." *Physics of Fluids* 14.12 (2002): 4206-4215.

Yüceil, K. Bülent, M. Volkan Ötügen, and Engin Arik. "Underexpanded sonic jets: A PIV study." *10th International Symposium on Application of Laser Techniques to Fluid Mechanics, Lisbon, Portugal*. 2000.

Zaman, K. B. M. Q. "Asymptotic spreading rate of initially compressible jets—experiment and analysis." *Physics of Fluids* 10 (1998): 2652. Print.

Zerkle, D. “NRC Update #1: Prediction of Supersonic Expansions Relevant to Debris Generations, LA-UR-00-2247.” A study prepared at Los Alamos National Laboratories. Print.